Topological Quantum Computing with Majorana Zero Mode Qubits: Theory and State of the Art

Martin Jay Caspe

A capstone project

submitted in partial fulfillment of the

requirements for the degree of

Master of Science

University of Washington

2020

Committee:

Professor Boris Blinov

Professor R. Jeffrey Wilkes

Program Authorized to Offer Degree:

Physics

University of Washington

Abstract

Topological Quantum Computing with Majorana Zero Mode Qubits:
Theory and State of the Art

Martin Jay Caspe

Professor R. Jeffrey Wilkes, Chair
Professor Boris Blinov
Physics

Topological Quantum Computing (TQC) has been proposed as a strong candidate for universal quantum computation, due to its inherent capability for fault-tolerance in the form of error detection and correction, and robustness against decoherence. Specifically, over the last decade significant investment has been directed toward research into materials that support Majorana Zero Mode (MZM) states for use as qubits, and the logic gates that allow them to be fused and braided together to encode data and allow them to evolve in quantum calculations. This capstone project first reviews the basics of Quantum Computation (QC), then explains the Physics of TQC, developing the theory conceptually with minimal recourse to mathematical calculation. Next, this understanding is applied to Majorana qubits specficially. Finally, the contemporary literature of MZM materials and gates is reviewed, along with near-term next steps toward realization.

TABLE OF CONTENTS

Page

Chapter 1

INTRODUCTION TO QUANTUM COMPUTING

Quantum Computing (QC) promises massive improvements over classical computing in solving certain types of problems, notably search, factorization, and modeling of quantum mechanical and chemical engineering systems. By encoding information in quantum mechanical "qubit" states rather than in classical "bits" of 1's and 0's, the properties of superposition and entanglement can be exploited, and vast quantities of information can be stored in just a few hundred or thousand qubit sites.

However, the required quantum states and resulting evolution of the system are highly susceptible to corruption from environmental noise. Typically experimental systems are built in cryogenically cold tanks—close to absolute zero—to limit thermal effects and avoid decoherence.

Topological Quantum Computation (TQC) is a promising theoretical sub-field which seeks to exploit exotic states of matter called "anyons." Anyons emerge as quasiparticle excitations of two-dimensional lattice structures of elementary particles constrained to a surface. Information is encoded when these anyonic quasiparticles are created, fused, rotated, or exchanged with each other. In general, the resulting states do not depend on the specific paths the particles have moved along, but only their topology. In theory, this topological robustness can be used as inherent error detection and correction, making TQC an attractive contender in the hunt for universal quantum computing capability.

Within the category of TQC, there are many theoretical models. Some have been proven to be capable of fully universal calculation (i.e. Turing-complete), while others are not. In the discussion below, we focus on the example of the Ising anyon model, which is not by itself Turing-complete, but can be made so with the addition of a measurement operation.

Majorana Zero Modes are physical examples of Ising anyons, and the subject of significant research and investment. These quasiparticle excitations come in both Abelian and

non-Abelian flavors, and exhibit the same statistics as the class of fermions hypothesized by Ettore Majorana in 1937.

1.1 Origins

Richard Feynman in his keynote address to the First Conference on the Physics of Computation at MIT in 1981, famously lays out the case for using "Quantum Computers" to simulate physical systems. He proposes a "guess: that every finite[1] quantum mechanical system can be described exactly, imitated exactly, by supposing that we have another system such that at each point in space-time this system has only two possible base states" [1]. These two-state "points" are now called "qubits," in analogy to the "bits" of conventional computers. Feynman then lays out quantum mechanical operators which could describe each lattice point in such a system: annihilation and creation operators for a lattice where each site is either occupied or unoccupied and the Pauli σ matrices for systems where each site is occupied by spin-one-half particles. He posits that such a machine could simulate *any* system of elementary particles with integer spin (*bosons*), although he has not yet worked out whether the two-state lattice is general enough to simulate system of particles of 1/2-integer spin (*fermions*). While the section describing this new Quantum Computer is quite short, the remainder of the address is dedicated to proving that quantum systems *cannot* be simulated on a classical computer, even if such a computer is enhanced with the capability to generate probabilistic answers. In this seminal work, Feynman both lays out a roadmap for quantum computing, and also proves the motivation for it.

In the mid-1990's two now-famous algorithms were published, that further demonstrated the immediate utility of a universal Quantum Computer, if only one could be built. In 1994 David Shor published his algorithm for quantum factorization and in 1996 Lov Grover published his search algorithm, with important and immediate applications in cryptography and data analysis, respectively. Indeed, Shor's algorithm would be capable of compromising the RSA encryption [2][2] commonly used for Internet security. The publication of these algo-

[1] Feynman also imposes the assumption of discretized space and time

[2] Assertions and figures in the remainder of Chapter 1 are broadly drawn from [2], if not othewise cited.

rithms led to significant interest and investment in QC hardware and algorithm development over the past 25 years.

1.2 Building Blocks: Qubits and Gates

The basic element of QC is the quantum bit, or *qubit*. Analogous to the *bit* of classical computers which can take the values 0 and 1, qubits are quantum mechanical objects that can take states represented in Dirac bra-ket notation as $|0\rangle$ and $|1\rangle$. In order to achieve the hoped for *quantum speedup*, qubits must be able to sustain superposition states, and entanglement, as would be expected of quantum objects. The mechanisms used to place qubits in superpositions of basis states, entangle them together, and generally manipulate them are called *gates*.

The study of QC breaks broadly into two disciplines which can be thought of as theoretical and experimental. Theoretical research includes the work of Shor and Grover and many others, in the search for algorithms that exploit the strange properties of quantum physics to achieve quantum speedup. Theorists also propose new materials and architectures that might enable QC. Qubits are treated mathematically as vectors, which are logical abstractions of the qubit states. Gates are represented as unitary matrices that act on the qubit vectors to affect transformations. Superposition and entangled states are represented as linear combinations of the basis vectors, as shown below. Theorists use the mathematics of quantum mechanics to develop algorithms and proofs, and evaluate potential models according to known physical properties and constraints.

A few simple examples are shown here to give a flavor of the mathematical language. As mentioned above, qubits are two-state quantum objects. When a qubit is measured it is always found to be in one state or the other. It is convenient to simply label one state $|0\rangle$ (for example, the ground state), and the other $|1\rangle$ (for example, the excited state). These vector labels can be assigned to orthogonal, normal column vectors:

$$|0\rangle = \begin{pmatrix} 1 \\ 0 \end{pmatrix}, \qquad |1\rangle = \begin{pmatrix} 0 \\ 1 \end{pmatrix}.$$

When multiple qubits are present (as they would be in any real application), the overall system state is represented by the tensor product of the individual states. This notation

is often omitted, so the overall state of a two qubit system with both initialized in the $|0\rangle$ state could be written:

$$|0\rangle \otimes |0\rangle \equiv |0 \otimes 0\rangle \equiv |00\rangle = \begin{pmatrix} 1 & \begin{pmatrix} 1 \\ 0 \end{pmatrix} \\ 0 & \begin{pmatrix} 1 \\ 0 \end{pmatrix} \end{pmatrix} = \begin{pmatrix} 1 \\ 0 \\ 0 \\ 0 \end{pmatrix}$$

Before it is measured, a qubit $|\psi\rangle$ exists in a superposition state which is a linear combination of its basis states:

$$|\psi\rangle = \alpha\,|0\rangle + \beta\,|1\rangle\,, \qquad |\alpha|^2 + |\beta|^2 = 1$$

where we are careful to maintain normalization. Linear coefficients α and β are in general complex, and therefore have an amplitude and a phase.

Every QC algorithm begins by physically initializing the qubits into a known state, and and then operating some combination of single-qubit and/or multiple-qubit gates. A simple and common example of a single-qubit gate is the Hadamard gate, which in matrix notation takes the form

$$H = \frac{1}{\sqrt{2}} \begin{pmatrix} 1 & 1 \\ 1 & -1 \end{pmatrix}.$$

Applying the Hadamard gate to the basis states $|0\rangle$ and $|1\rangle$ *rotates* them to an equal superposition state:

$$|\phi_0\rangle = H\,|0\rangle = \frac{1}{\sqrt{2}} \begin{pmatrix} 1 & 1 \\ 1 & -1 \end{pmatrix} \begin{pmatrix} 1 \\ 0 \end{pmatrix} = \frac{1}{\sqrt{2}} \begin{pmatrix} 1 \\ 1 \end{pmatrix} = \frac{1}{\sqrt{2}}(|0\rangle + |1\rangle)$$

$$|\phi_1\rangle = H\,|1\rangle = \frac{1}{\sqrt{2}} \begin{pmatrix} 1 & 1 \\ 1 & -1 \end{pmatrix} \begin{pmatrix} 0 \\ 1 \end{pmatrix} = \frac{1}{\sqrt{2}} \begin{pmatrix} 1 \\ -1 \end{pmatrix} = \frac{1}{\sqrt{2}}(|0\rangle - |1\rangle)$$

After all the gates are applied, the result is obtained by performing a measurement, or *readout* of the system. This results in collapse of the superpositions into either a $|0\rangle$ or $|1\rangle$ for each qubit, the usual wave function collapse seen in quantum mechanical systems. In the example above, if $|\phi_0\rangle$ were to be measured after application of the Hadamard, the result would be $|0\rangle$ or $|1\rangle$, with equal probability.

1.3 Physical Realizations

Many two-state quantum objects can be used as qubits. Feynman's seminal address in 1981 already implicitly included two potential candidate systems for realizing a physical system of two-state quantum objects: a lattice of sites either occupied or unoccupied with creation and annihilation operators to change state, and a lattice of spin states with the Pauli matrices as gate operators. Polarization of single photons, single electrons of spin up or spin down, excitation states of trapped ions, the current in superconducting Josephson junctions, exciton energy within quantum dots, and even individual atoms within molecules subjected to NMR pulses are all two-state qubit systems which have been studied and built in the lab, with various success.

Efficacy of a physical implementation is judged against the *di Vincenzo criteria*, which are considered the minimum requirements for universal computation [2]:

1. Scalable. The system must be capable of supporting many well defined qubits;
2. Initializable. The qubits must be able to be initialized in the state $|0\rangle$;
3. Coherence time. The qubits must remain isolated from the environment and in their coherent states long enough to usefully complete calculations;
4. Universal set of quantum gates. The system must include mechanisms to implement at least a minimal set of gates to ensure Turing-complete calculation is possible;
5. Readable. There must be a method to readout the final result of the calculation;

Different systems have different strengths and weaknesses, and it is instructive to consider how they stack up against the criteria. Two well studied systems are described below, and the extent to which each meets de Vincenzo's criteria is a snapshot of its state of development and potential as a future universal QC platform.

1.3.1 Trapped Ions

Qubits made of trapped ions have been extensively studied. Because they are electrically charged, it is possible to spatially contain them using combinations of constant and oscillating electromagnetic fields, for example within a *Paul trap*. The ions are caught within a harmonic potential of the form $V(x, y, z) = \frac{1}{2}M(\omega_x^2 x^2 + \omega_y^2 y^2 + \omega_z^2 z^2)$, where M is the mass

of the ion, $\mathbf{r} = (x, y, z)$ is the position, and ω_i are the oscillating trap frequencies in each dimension. Modern traps are implemented using microfabrication techniques such as those used to manufacture MEMS devices, with the goal of attaining the reproducibility of the CMOS process [3].

The $|0\rangle$ qubit state is defined as the electronic ground state, and the $|1\rangle$ state is an electronically excited state, chosen for its stability (˜1 sec). Initialization is accomplished by optically pumping the ions to the desired electronic state, and single qubit gates such as the Hadamard gate described in Section 1.2 are accomplished by shining precisely timed laser pulses at the target qubit. For example, to rotate a qubit state from $|0\rangle$ to $|1\rangle$, a π *pulse* of duration $t = \pi/\Omega$ is used, where Ω is the Rabi frequency of the atomic transition. If a pulse of half that duration is used, the qubit is placed in a superposition of states:

$$|0\rangle \xrightarrow{t=\pi/\Omega} |1\rangle\,, \qquad |0\rangle \xrightarrow{t=\pi/2\Omega} \tfrac{1}{\sqrt{2}}(|0\rangle + |1\rangle)$$

This requires pulse durations on the order of 100 ns. Sources of error in these rotations are the precision of the pulse timing, stability of the laser light in brightness, frequency, and phase, and consistency of the light path to the target ion. As of 2016, pulse precision was good enough that error in the single qubit rotations was not a limiting factor toward realization of QC [4].

In addition to their electrical state, trapped ions have motional states due to their harmonic motion within the trap. QC architectures harness this motional degree of freedom to couple the electonic states of neighboring qubits. This is how the qubits are entangled to create the two-qubit logic gates that are required for universal computation.

Trapped ions for QC have the advantage of long electrical stability times, ease of detection for readout, and high demonstrated accuracy. However, short coherence times of the motional states, controlling heating of the qubits, and difficulties in scaling still need to be overcome.

1.3.2 Superconducting Josephson Junctions

Where trapped ion systems require engineering control at the single-atom level, superconducting qubits are macro-scale quantum objects, and some of them exhibit macro-scale

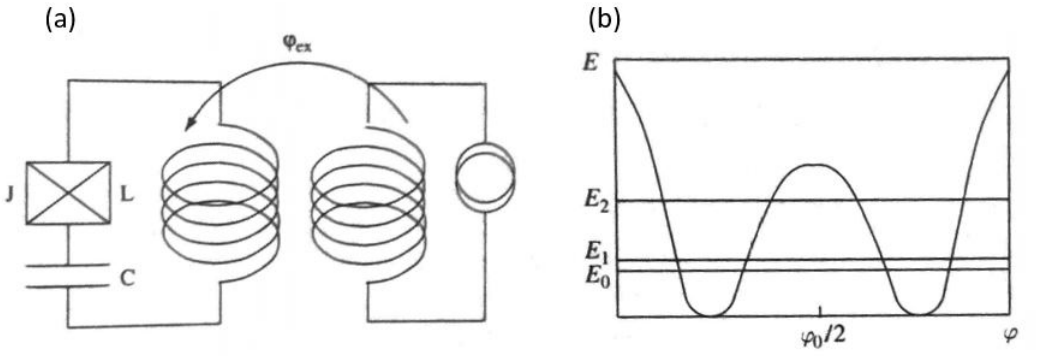

Figure 1.1: Superconducting Josephson junction *flux qubit* (a) Circuit with capacitor C, Josephson junction J, two inductors coupling external flux ϕ_{ex}, and alternating power source; (b) Potential $U(\phi)$, showing two distinct states at low energies E_i, with $\phi_{ex} = \phi_0/2$.

states. Superconducting qubit architecture drives the famous prototype quantum computers of IBM and Google.

A simple superconducting harmonic oscillator can be constructed from an inductor and a capacitor. The energy gap between its states is too small, however,and two distinct levels cannot be uniquely isolated. Addition of Josephson junctions, constructed by sandwiching insulating material between two superconductors, introduces nonlinearities into the circuit. The oscillator becomes *anharmonic* and capable of supporting the requisite two distinct states.

Three different types of superconducting qubits have been demonstrated: *flux qubits*, *charge qubits*, and *phase qubits*. Many prospective architectures are hybrids of these, such as the *quantronium* charge-phase qubit. In recent years, the *Transmon*, a version of the charge qubit designed to have reduced sensitivity to charge noise, has received significant attention [5].

To generate flux qubits, for example, a loop circuit (Fig. 1.1(a)) consisting of an inductor, capacitor and Josephson junction, is inductively coupled to a driving voltage through external flux ϕ_{ex}. This gives rise to the potential $U(\phi)$ (Fig. 1.1(b)). At low energy levels, $U(\phi)$ has two distinctive wells, corresponding to easily measurable current on the order of 1 μA flowing in the clockwise (assigned $|0\rangle$) or counter clockwise (assigned $|1\rangle$) direction

around the loop. Note that at low energy levels $E_1 - E_3$, the system is classically forbidden from changing state. However, as a quantum system, there is a probability of tunneling from one well to the other, resulting in capability for superposition states.

Single-qubit gates are realized by time-measured microwave frequency pulses (similar to the optical pulses used in trapped ion qubit control), coupled either through radiation or conduction. Qubits are coupled together in various ways depending on architecture, and many designs depend on coupling via a microwave cavity.

Superconducting Josephson junction qubits are designed and produced using well understood microfabrication and lithographic techniques. They depend on fabricated circuit elements, which can be freely modified and adjusted to yield the desired responses, like "artificial atoms" [5]. In recent years, the coherence times of superconducting qubits has increased substantially, but they remain quite sensitive to readout, with accuracy precision on the order of 1/1000, and require microwave frequency signal control that is not yet well developed. As with all physical realizations, scaling is an open problem and an active area of research.

1.3.3 Decoherence

One of the di Vincenzo criteria for realizable qubits is that they must have sufficiently long coherence times. According to Le Bellac, "The Enemy Number One of a quantum computer is *decoherence*, the interaction of qubits with the environment which blurs the delicate linear superpositions" [2]. When decoherence occurs, the wave function of the qubits becomes mixed with the wave function of the environment, and the phase information (for example, encoded in coefficients α and β from Section 1.2) is lost.

To lengthen coherence times, qubits must be isolated from their environment. Quantum computers are kept at micro-Kelvin temperatures using various cooling schemes, depending on the particular physical realization. A key motivation for topological qubits is that they are inherently resistant to decoherence, as discussed below.

1.4 Quantum Speed-up

The allure of QC is that certain types of calculations can be done much faster than conventional computers. However the source of this "quantum speedup" is subtle. For some problems, such as search and integer factorization mentioned above, quantum algorithms have been found and logically proven to be faster than their classical equivalents (to a certain probabilistic precision). Many other algorithms have been proposed in more specialized fields, such as modeling quantum many-body problems. It is hoped that QC will be able to solve whole classes of difficult problems much faster than classical computers, although this is yet to be proven.

Quantum supremacy, sometimes called *quantum computational advantage*, means that a quantum computer can complete a calculation demonstrably faster than a classical computer. In 2019, Google announced their superconducting transmon-based "Sycamore" computer had achieved quantum supremacy "in the task of sampling the output of a pseudo-random quantum circuit" [6]. More recently, in December of 2020, a group from China also claimed quantum computational advantage as they published results of Gaussian boson sampling by a photon-based quantum computer: "The photonic quantum computer generates up to 76 output photon clicks, which yields...a sampling rate that is $\sim 10^{14}$ faster than using the state-of-the-art simulation strategy and supercomputers" [7].

While boson sampling is an esoteric application, these recent announcements illustrate great strides toward the promise of QC.

Chapter 2

TOPOLOGICAL QUANTUM COMPUTING

Topological Quantum Computation (TQC) attempts to solve the problems of decoherence and fault-tolerance by exploiting exotic configurations and properties of materials. The theory is quite distinct from the methods and equations used for other realizations of QC. It depends on states that arise within quasiparticles called *anyons*. These localized excitations of ensembles of elementary particles are constrained to two dimensions. Information is encoded in the anyon phases when these particles are physically exchanged, or encircled, around each other in intricate braiding patterns called *worldlines*. This chapter starts from basic principles and goes into detail in several examples, to impart the flavor of how these novel ideas build from elementary particles to complex systems capable of universal computation.[1]

2.1 Exchange Statistics

TQC gets its name from the use of topological states as qubits. *Topology* is "a branch of mathematics concerned with those properties of geometric configurations...which are unaltered by elastic deformations (such as a stretching or a twisting)...." [9]. TQC seeks to implement qubits such that their quantum state "properties" are topologically protected under adiabatic (smooth) transformations, and therefore can be placed in superposition states, selectively entangled, and physically moved about without suffering from decoherence or bit errors like conventional qubits. In other words, TQC seeks to create a system where the gate operations are analogous to the elastic deformations of topology, and the properties which are unaffected are the coherence and the lack of errors, while still meeting the di Vincenzo criteria for a universally programmable computer. The enabling concept

[1]The development in Chapter 2, as well as all the figures, are broadly drawn from [8] if not otherwise cited.

for this technology is that of exchange statistics.

All elementary quantum particles can be classified as bosons or fermions.[2] Bosons, such as photons, or isotopes with even numbers of charges, have integer spin and obey *Bose statistics*. A direct result of this is that they can have identical quantum numbers: Many bosons can occupy the same state—and therefore can be formed into Bose-Einstein condensates. On the other hand spin-1/2 fermions, such as electrons, quarks, and any isotope with odd numbered charge, cannot occupy the same quantum state, but must obey the Pauli exclusion principle. Exchange statistics apply to the state expression of the entire system. In an ensemble of bosons, if two particles are exchanged—i.e. their physical locations are swapped—the state of the system is unaffected. In an ensemble of fermions on the other hand, if two particles are exchanged the state expression of the system takes on the opposite sign. This is denoted as acquiring an overall phase of -1. Further, it does not matter what path the particles take as they are exchanged. The +1 or -1 phase is one of the topological properties that is not affected by deformations of the path taken by the particles during the exchange, so only their initial and final positions matter.

In both cases, if the exchanged particles are exchanged again, the system is returned to the original state:

$$|\Psi_b\rangle \xrightarrow{\text{exchange}} +1\,|\Psi_b\rangle \xrightarrow{\text{exchange again}} |\Psi_b\rangle$$
$$|\Psi_f\rangle \xrightarrow{\text{exchange}} -1\,|\Psi_f\rangle \xrightarrow{\text{exchange again}} |\Psi_f\rangle$$

If we define an exchange operator C_{ex}, this can be expressed more compactly:

$$C_{ex}\,|\Psi_f\rangle = -1\,|\Psi_f\rangle$$
$$C_{ex}C_{ex}\,|\Psi_f\rangle = |\Psi_f\rangle$$

This is an unsurprising result: It makes sense that swapping two particles and swapping them again would leave the system unchanged and this is exactly what happens in 3 dimensions. It is important to note that a double exchange is equivalent to moving one particle

[2]Bose statistics, or the Bose-Einstein distribution, were first introduced in a jointly authored paper in *Zeitschrift für Physik* in 1924. Fermi-Dirac statistics, or Fermi-Dirac distribution, was introduced in separate papers by Fermi and Dirac in *Rendiconti Lincei* and *Proceedings of the Royal Society* in 1926 respectively. They are governed by the following expression: $\bar{n}_i = \frac{g_i}{e^{(\epsilon_i-\mu)/k_BT}\pm 1}$ with the -1 in the denominator applying to bosons, and the +1 applying to fermions.

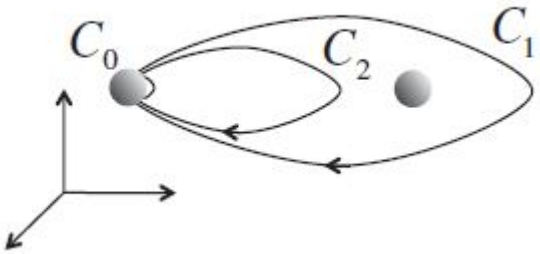

Figure 2.1: Path C_1, which shows the left particle encircling the right particle, can be smoothly deformed in three dimensions into path C_2, which no longer encircles the right particle, and ultimately to the trivial path C_0, which is no movement at all. Because it is possible to smoothly deform one path into the other, their wave functions must be identical.

completely around the other. (To picture this, imagine the swap from the reference frame of one of the particles).

2.2 Topological Exchanges

Under certain conditions, particles can be engineered to take on more complex phases than ± 1 when exchanged. The resulting states are topologically protected, in that the induced phases depend only on the topological characteristics of the process: they do not depend on the specific path taken, the speed of exchange, or other parameters.

Consider two particles in 3 dimensions (see Fig. 2.1). One is held steady, and the other is moved in path C_1 around the first. The path can be deformed smoothly in space so that instead of encircling the particle, it makes a circle C_2 around the empty space beside the particle. Shrinking it further, always making only local deformations, the path is reduced to the trivial case where the particle is not actually moved at all, C_0. We assert that the wave function of the system in each of the three cases must be the same:

$$\Psi(C_1) = \Psi(C_2) = \Psi(C_0)$$

This is only possible in 3 spatial dimensions, where the path can deform over or under the stationary particle, and it matches our results for twice swapping bosons and fermions in Section 2.1 above.

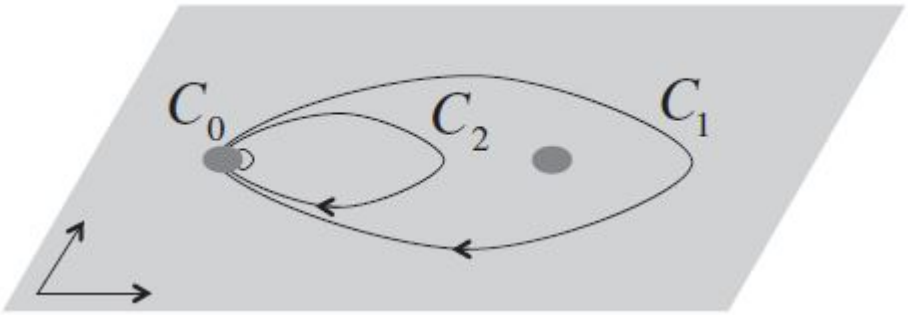

Figure 2.2: When constrained to two-dimensions, path C_1 is no longer topologically equivalent to C_2 (which is equivalent to the starting position C_0), so it may be possible to find a system which acquires an arbitrary phase when path C_1 is traversed.

On the other hand, if the system is constrained to two dimensions (as in Fig. 2.2), the path C_1 encircling the particle *cannot* be smoothly deformed to the original state C_0. Rather, it must be cut and re-joined, or must pass through the second particle, or in some other way dramatically have a different character. In two dimensions, these two cases are topologically distinct, as described in Sections 2.2.1 and 2.2.2 below.

2.2.1 Aharonov-Bohm Effect

While it is intuitive that returning an ensemble to its original configuration should not change the state, there are well-studied systems where this is not the case. In a demonstration of the Aharonov-Bohm effect[3], an electrically charged particle is adiabatically moved in a loop around a surface that contains magnetic flux, constrained by a solenoid (see Fig. 2.3). Even though the particle cannot interact directly with the flux, the movement through the vector potential $\mathbf{A}$ imparts a non-trivial phase $\phi = \frac{q}{c\hbar}\Phi$ to the state of the particle. As long as the amount of encircled flux Φ does not change and the path is traversed adiabatically, the phase ϕ does not depend on the trajectory or the speed, but only on the number of times the flux is encircled. The phase factor $e^{i\phi}$ is applied to the Eigenvector solution

[3]In the development of Electrodynamics, such demonstrations provided evidence that the vector potential $\mathbf{A}$ is an actual, physical phenomenon, rather than a mathematical convenience

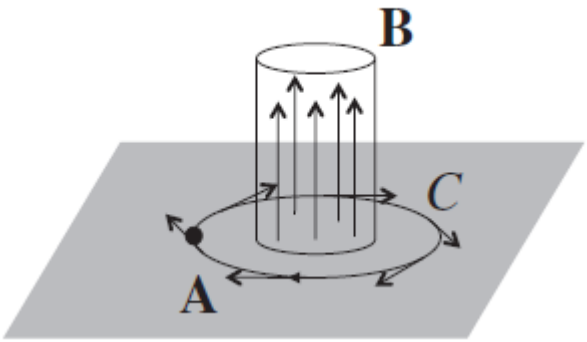

Figure 2.3: Particle is adiabatically moved along path C through vector potential **A** created by magnetic field **B**, which is contained within an impenetrable solenoid. Particle is imparted with a non-trivial phase $\phi = \frac{q}{c\hbar}\Phi$ which is topological in that it is not path dependent.

of Schrödinger's equation for the particle, which must be squared to yield the probability function. Squaring the generally complex-valued phase factor yields unity, so the phase is not directly measurable. However, the relative phases of different particles can be indirectly observed, and they are the key to encoding information for topological quantum calculations.

2.2.2 Anyons and Topological Phase Factors

The goal of TQC is to find a physical implementation where such non-trivial phases can be exploited, and used to encode information. To have potential to work in this way, qubits must be least two-state quantum objects, constrained to two dimensions, and

The quantum entities with potential to meet these criteria for topological qubits are called *anyons*. This term was coined because of their exchange statistics: unlike bosons, which take only phase +1, or fermions, which take only phase -1, anyons can in theory take any arbitrary phase under exchange, as described below.

The first criterion for anyons is that they are constrained to two dimensions. Elementary particles are inherently three-dimensional, even when constrained to motion in two

dimensions. However, it is possible to envision a particle with spatial location $\boldsymbol{r} = (x, y, z)$ subjected to a potential of the form

$$V(\boldsymbol{r}) = V_{xy}(x, y) + V_z(z)$$

who's wave function can be shown by separation of variables to be

$$\Psi(\boldsymbol{r}) = \Psi_{xy}(x, y)\Psi_z(z)$$

Here, $\Psi_{xy}(x, y)$ satisfies the two-dimensional Schrödinger equation of the particle subjected to $V_{xy}(x, y)$ and $\Psi_z(z)$ satisfies the one-dimensional Schrödinger equation subjected to $V_z(z)$. We require a system where there is a substantial energy gap ΔE between the ground state and the first excited state of $\Psi_z(z)$. This means, if initialized in the ground state, the system will be energetically incentivized to remain there, and if the environment is carefully controlled, $\Psi_{xy}(x, y)$ can be considered the effective wave function of the particle: $\Psi(\boldsymbol{r}) \to \Psi_{xy}(x, y)$. This wave function satisfies the constraint on two-dimensionality required for topological properties to emerge. Further, we are looking for a similar energy gap between the ground state and first excited state of the two-dimensional wave function, to ensure robustness to perturbations and temperature fluctuations. These exotic constraints cannot be met by elementary particles, but could potentially be satisfied by careful engineering of *quasiparticles*.

Quasiparticles are localized excitations of an ensemble of constituent particles. They arise in crystals, lattices, and other configurations where complex structures give rise to collective phenomena that can be characterized similarly to particles (see Fig. 2.4). For example, sound travels through a solid by coherent vibrations of the lattice molecules, which obey wave mechanics as if they were actual particles, and are called *phonons*. Phonons are the "fictitious particles...each endowed with with energy $\hbar\omega$ associated with [a quantum] oscillator of classical frequency ω" [10]. Quasiparticles can be described by their own Hamiltonian, with associated creation and annihilation operators, just like any quantum particles.

All prospective realizations of topological qubits rely on this concept: Anyons must be quasiparticles. To develop a deeper intuition of how anyons acquire topological phases, let

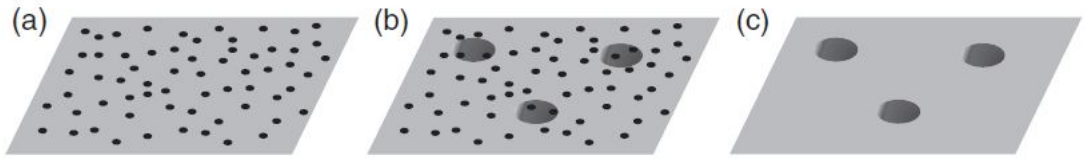

Figure 2.4: Cartoon of quasiparticles emerging from an ensemble of elementary particles. (a) A system of constituent elementary particles confined to a two-dimensional surface; (b) Quasiparticles, which are localized properties of the system, shown together with constituent particles; (c) Quasiparticles constrained to two dimensions, shown as often conceived, with constituent particles not individually considered

us consider the example of two quasiparticles which are designed to have charge q and an inherent magnetic dipole with associated flux Φ, labeled 1 and 2 in Fig. 2.5(a). For this discussion, the underlying ensemble of constituent particles is not relevant, and the Physics is developed at the quasiparticle level of abstraction. When anyon 1 is circulated around anyon 2 along path C, we have an exact example of the Aharonov-Bohm effect described in Section 2.2.1, with the charge q of anyon 1 circulating the flux Φ of anyon 2, and we know the system acquires a phase of $\phi = \frac{q}{c\hbar}\Phi$. Suppressing c and $\hbar$ for simplicity, this phase factor $e^{iq\Phi}$ is topological in that it does not depend on details of the path C (such as the trajectory or speed), but only on the number of circulations. In the same action, the flux Φ of 1 has encircled the charge q of 2, imparting another phase factor $e^{iq\Phi}$, for a total of $e^{2iq\Phi}$ for the system of two anyons under double exchange along loop C.

Similarly, anyonic spin can be encoded in the phase. Fig. 2.5(b) shows the anyon rotating around itself. In this case, if the charge q is contained in a ring around the flux Φ, a rotation of 2π imparts a phase factor of $e^{iq\Phi}$. Looked at the other way, when q or Φ are altered, an effective spin s is imparted to the anyon, through the phase factor $e^{i2\pi s}$, where $s = \frac{q\Phi}{2\pi}$.

This example uses the analogy of the Aharonov-Bohm effect to show how theoretical anyons with charge q and magnetic flux Φ take on non-trivial phases under exchange and rotation operations. As previously noted, the overall phase factors are not measurable in real systems, because they square to unity when the expectation value is calculated:

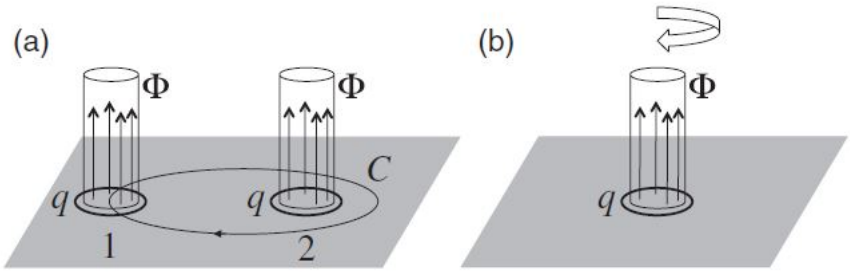

Figure 2.5: Anyon quasiparticles of charge q and magnetic flux Φ. (a) Anyon 1 with charge q is circulated around the flux Φ of anyon 2 along path C. The system acquires a phase of $\phi = 2iq\Phi$ due to Aharonov-Bohm effect. (b) Anyon is rotated around itself, acquiring a factor $e^{iq\Phi}$ for each 2π rotation due to its own charge q circulating its inherent flux Φ.

$$\langle\Psi|\, e^{-i\phi} A e^{i\phi}\, |\Psi\rangle = \langle\Psi|\, A\, |\Psi\rangle$$

Further, when multiple phase factors are applied, the order of operations does not matter:

$$e^{i\phi_1} e^{i\phi_2}\, |\Psi\rangle = e^{i\phi_2} e^{i\phi_1}\, |\Psi\rangle$$

An *Abelian group*[4] is one where the order of applying the group operation does not affect the outcome. In a word, commutation holds. Anyons which take on phase factors as in the previous example are therefore called *Abelian anyons*. It has been shown that universal quantum computation is not possible using Abelian anyons alone, although they may have applications in quantum memory and readout, and they are certainly useful as a conceptual tool.

2.2.3 Non-Abelian Anyons

A more exotic and complicated type of anyons has been theorized, which *could* lead to universal computation. When these are exchanged, their statistics are characterized by operation of a unitary matrix on the state, rather than a complex phase factor. Matrices do not in general commute, hence the designation *non-Abelian* anyons. To be possible, the wave function that describes the system of quasiparticles must be one of a number of different states of the same energy—it must be part of a degenerate subspace of states. Further, the

[4]So named in honor of Niels Henrik Abel, Norwegian mathematician, 1802-1829

states must be indistinguishable locally. Exchanging two non-Abelian anyons then results in a linear transformation from one degenerate state to another, by definition not changing the energy of the overall system. In order to ensure a valid statistical transformation, the exchange must not be detectable by looking at the anyons individually. The remainder of this chapter discusses how such anyons could be used as qubits for TQC, and Chapter 3 explores one potential technology in detail.

2.3 Worldlines and Braiding

We have seen in Section 2.2.2 one detailed example of how the exchange of two Abelian anyons can impart a non-trivial phase to the overall system, and mentioned in Section 2.2.3 that exchange of non-Abelian anyons can be represented mathematically as operation on the system by a unitary matrix. This section will cover how anyon creation, exchanges, and fusions are depicted using *worldline* notation, abstraction of fusion and exchange operations as F and R matrices, and go into some detail about the Ising model, which also applies to the Majorana Modes of Chapter 3.

2.3.1 Create, Exchange, Fuse

Various anyonic models have been explored, involving different species of anyon quasiparticles, and different exchange properties. In general, we can label the species $1, a, b, ...$, where 1 refers to the vacuum, or null state, with no anyons in the system, a is the first species to be defined within the particular model under discussion, and so on.

Computation with anyons involves several steps:

1. Creating the particle and anti-particle from vacuum
2. Selectively exchanging anyons to encode data and gate operations as the system state
3. Selectively merging anyons together. Together with exchange, this is the *braiding* process.
4. Final merging to readout the result

These steps are visualized graphically in *worldline* diagrams. These are representations of the history of each anyon in an ensemble, and show the two dimensional spatial relationships,

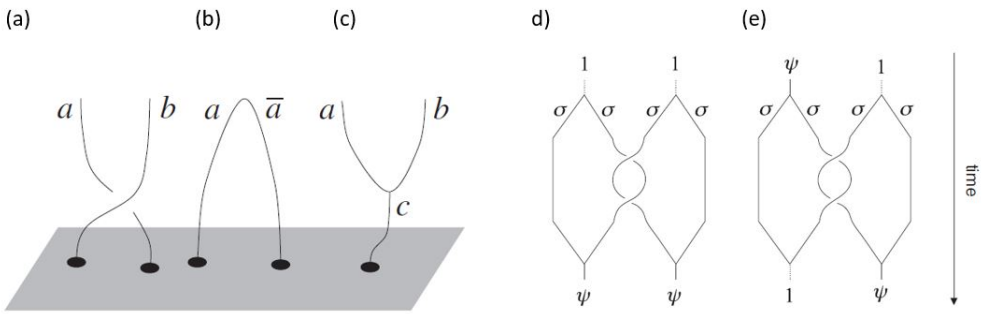

Figure 2.6: (a-c) Generic worldlines showing (a) exchange of particles a and b; (b) creation of particle a and antiparticle $\overline{a}$ from the vacuum; (c) merging of particles a and b into c; and (d-e) Ising anyon examples showing (d) creation of two pairs of σ anyons, a double exchange, and two fusions to yield two ψ fermions; (e) one pair of σ anyons created from vacuum, and one pair from ψ fermion, double exchange, and two fusions to yield a teleportation of the original ψ fermion from one pair to the other

.

evolving from the top of the diagram to the bottom (or left to right) in time. Figure 2.6(a)-(c) shows the major elements of anyon braiding with generic particles a, b, and c: (a) is the simple exchange of particles a and b, (b) shows creation of particle a and its antiparticle $\overline{a}$ from the vacuum, and (c) illustrates the merging of a and b to form c.

When describing a particular model, the first definition should be which species of anyons are involved, and description of their fusion characteristics. These characteristics can then be represented mathematically by a *fusion matrix*, or F matrix, and an *exchange matrix*, or R matrix. These matrix operators are combined into a *braid matrix*, or B matrix, which describes how a braid operates on a system state. To clarify these concepts and notation, we will develop the example of the Ising anyon model.

2.3.2 Ising Anyon Model

We will now show how the F, R, and B matrices correspond to the non-trivial evolution of the Ising anyon model shown in the worldlines of Fig. 2.6 (d). The intent of this section is to delve into sufficient detail to convey the usefulness of worldline diagrams, how fusion

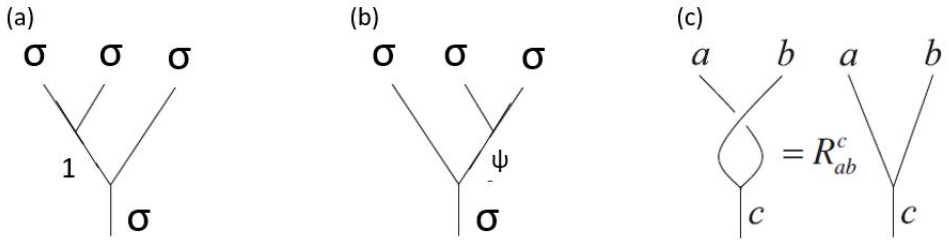

Figure 2.7: Illustration of F and R matrix action. Ways to fuse three σ anyons: (a) $\sigma \times \sigma = 1$ interim product, then $1 \times \sigma = \sigma$; (b) $\sigma \times \sigma = \psi$ as the interim product, then $\sigma \times \psi = \sigma$. The total fusion channel is σ; (c) Exchanging a and b, followed by fusing into c is equivalent to fusing a and b into c, rotated by phase R.

rules relate to the mathematical formalism of the fusion, exchange, and braiding matrices, and give a sense of how braiding results in state manipulation.

The Ising model has three species of anyon: the vacuum, 1; the non-Abelian anyon, σ; and the fermion, ψ. The fusion rules describe what results when any two species are fused. Combining two σ anyons will result in either vacuum, or fermion; fusing σ with ψ fermion gives σ, as if the ψ is absorbed by the σ; and fusing two fermions results in vacuum. Symbolically, these rules are represented as:

$$\sigma \times \sigma = 1 + \psi, \quad \sigma \times \psi = \sigma, \quad \psi \times \psi = 1$$

In addition, fusing either σ or ϕ with the vacuum is equivalent to the identity operation (i.e. $\sigma \times 1 = \sigma$). Further, these fusion rules are time reversible, so for example, two σ anyons can be created from either the vacuum, or ψ, as seen in Fig. 2.6 (d,e).

From these rules, it is possible to derive[5] the F matrix and R matrix operators which describe the fusion and exchange characteristics of the system. We consider the fusion of $\sigma \times \sigma$, which takes the values of 1 or ψ. There are two distinct ways to combine three σ anyons, as shown in Fig. 2.7. The first fusion produces an interim product of either 1 (a) or ψ (b), and the second fusion returns σ in either case. These fusions are formalized in the $F^{\sigma}_{\sigma\sigma\sigma}$ matrix, where the upper σ index indicates the total fusion outcome, and the lower

[5]This derivation is beyond the scope of this project. For details, see [8]

three σ indices denote the starting particles to be fused:

$$F^{\sigma}_{\sigma\sigma\sigma} = \frac{1}{\sqrt{2}} \begin{pmatrix} 1 & 1 \\ 1 & -1 \end{pmatrix}.$$

The F matrix can be thought of as a rotation[6] between states with interim fusion products of 1 or ψ (Fig. 2.7(a,b)).

To describe the exchange of two particles, let us consider generic particles a and b, and think about the case where there is only one fusion outcome: $a \times b = c$. Then exchanging a and b is equivalent to a half rotation of c (see Fig. 2.7 (c)). Since the exchange is equivalent to rotation of a single particle, it can be described by a simple phase factor, and the matrix R is constructed with each possible fusion outcome c on the diagonal.

For the Ising anyon case in Fig. 2.6 (d), the exchanged particles are both σ, and the fusion outcome could be 1 or ψ. It turns out[7] that $R^{1}_{\sigma\sigma} = e^{-i\pi/8}$ and $R^{\psi}_{\sigma\sigma} = e^{i3\pi/8}$. The matrix with these values on the diagonal is then:

$$R_{\sigma\sigma} = e^{-i\pi/8} \begin{pmatrix} 1 & 0 \\ 0 & i \end{pmatrix}$$

Now let us consider how the F and R matrices combine to describe the B braiding matrix. We want to describe the double exchange of the two σ anyons shown in the middle of Figure 3.3(d) and (e). Call this state $|\sigma, \sigma\rangle$. These two σs do not have a fusion channel, so introduce an interim, "virtual" fusion by acting on the state with F, apply the double twist by acting twice with R, and back out the virtual fusion - it was just a computational

---

[6]Fusing three σ particles always results in a σ, but there is an interim outcome which can be either 1 or ψ. The state of the fusion process for each case, $|i\rangle$ can take either $|\sigma, \sigma \to 1\rangle \otimes |1, \sigma \to \sigma\rangle$, or $|\sigma, \sigma \to \psi\rangle \otimes |\psi, \sigma \to \sigma\rangle$. The $F^{\sigma}_{\sigma\sigma\sigma}$ matrix can be thought of as rotating between these basis states: $|1\rangle = F^{\sigma}_{\sigma\sigma\sigma} |\psi\rangle$. Incidentally, the resemlance of $F^{\sigma}_{\sigma\sigma\sigma}$ to the Hadamard operator of Section **??** is purely coincidental.

[7]Again, see [8] for derivation.

convenience. The steps to achieve the double exchange then look like this:

$$|\sigma,\sigma\rangle \rightarrow \text{original pair}$$

$$F^{\sigma}_{\sigma\sigma\sigma}\,|\sigma,\sigma\rangle \rightarrow \text{pair fused into new "virtual" anyon}$$

$$R_{\sigma\sigma}F^{\sigma}_{\sigma\sigma\sigma}\,|\sigma,\sigma\rangle \rightarrow \text{"virtual" anyon rotated once}$$

$$R_{\sigma\sigma}R_{\sigma\sigma}F^{\sigma}_{\sigma\sigma\sigma}\,|\sigma,\sigma\rangle \rightarrow \text{"virtual" anyon rotated again}$$

$$(F^{\sigma}_{\sigma\sigma\sigma})^{-1}R_{\sigma\sigma}R_{\sigma\sigma}F^{\sigma}_{\sigma\sigma\sigma}\,|\sigma,\sigma\rangle =$$

$$(F^{\sigma}_{\sigma\sigma\sigma})^{-1}(R_{\sigma\sigma})^2(F^{\sigma}_{\sigma\sigma\sigma})\,|\sigma,\sigma\rangle \rightarrow \text{"virtual" particle unfused, leaving } \sigma \text{ particles doubly exchanged}$$

Calculating the value of this matrix braiding operator B using the values of F and R developed above, we have:

$$B = F^{-1}R^2F = \frac{\sqrt{2}}{2}\begin{pmatrix}1 & 1\\ 1 & -1\end{pmatrix} e^{-i\pi/4}\begin{pmatrix}1 & 0\\ 0 & i\end{pmatrix}^2 \frac{1}{\sqrt{2}}\begin{pmatrix}1 & 1\\ 1 & -1\end{pmatrix} = e^{-i\pi/4}\begin{pmatrix}0 & 1\\ 1 & 0\end{pmatrix}$$

.

This example shows the correspondence between the σ exchanges in the worldline diagram in Fig. 2.6 (d) and (e), and B, the braiding matrix. The worldlines qualitatively record the history of the system, and the braiding operator B formalizes the mathematics. It is now easier to picture how a desired gate operation could be constructed from multiple anyon exchanges.

In order to use the Ising model for quantum computation, we can define a logical qubit with the two states, $|0_L\rangle = |\sigma,\sigma \rightarrow 1\rangle$ and $|1_L\rangle = |\sigma,\sigma \rightarrow \psi\rangle$. Each logical qubit requires four anyons to encode a superposition of the two intermediate fusion outcomes. Note that because these are just intermediate states, they obey the requirement mentioned in Section 2.2.3 that there must be a degenerate subspace of non-locally distinguishable states.

This chapter has described the Physics of anyons using the example of the Aharonov-Bohm effect, where a charged particle acquires a relative phase when it encircles a magnetic flux. We discussed how quasiparticles arise from an ensemble of constituent elementary particles, and how the wave function of these quasiparticles can be confined to two dimensions. Exchange statistics of bosons and fermions were described and the concept of anyons was developed, using the example of a pair of two-dimensional quasiparticles with a ring of

charge q and inherent flux Φ. The difference between Abelian and non-Abelian anyons was mentioned and the Ising model of non-Abelian anyons was used as an example to illustrate how worldlines illustrate the braiding operation, which is mathematically formalized in the F, R, and B matrices. Finally, we suggested a path toward creating logical qubits within the Ising anyon model, and using them for computation.

Chapter 3

MAJORANA ZERO MODES

In the last chapter, we developed the theory of anyons, exchange statistics and non-trivial phases with little reference to physical systems that could support these exotic states. Now we will apply this theory to the specific case of Majorana quasiparticles which may form at the endpoints of one-dimensional "quantum wires," and build from this abstract concept to the concrete reality of microfabricated prototypes in the lab. This will lead us to a description of zero-energy Majorana pairs called *Majorana Zero Modes*, (MZM).

3.1 Theory of Majoranas in Nanowire

We will explore what Majorana particls are, the very specific configurations where they may arise, and how they may be braided and manipulated to form gates.

3.1.1 What is a Majorana?

In 1937, Ettore Majorana developed the theory of fermionic particles that are their own antiparticle [11]. Majorana's contribution is a modification of Dirac's now-famous wave equation which explains spin-1/2 particles. Dirac's equation includes both real and complex numbers, which he considered a feature, and which led to explanation of the positron. Majorana asked whether it was possible to write down an equation for spin-1/2 fields that only involved real numbers, and the Majorana Equation was the result. He was encouraged to publish this "big idea" in 1937, and disappeared mysteriously and tragically soon after.[1]

To date, no elementary Majorana particles have been found, although perhaps the neutrino is a candidate, as Majorana himself originally speculated. The field of supersymmetry predicts a number of "superpartner" spin-1/2 particles (such as the *photino*), which

[1]Majorana's mysterious and romantic disappearance has been the subject of much speculation. Perhaps he was his own antiparticle and annihilated himself!

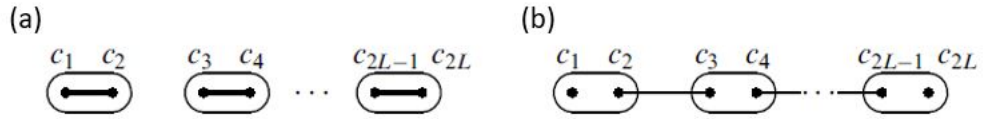

Figure 3.1: Kitaev's nanowire toy model; (a) Majoranas c_i (represented as dots) paired together at fermion sites (ovals); (b) Majoranas c_i paired *across* fermion sites, leaving unpaired Majoranas at the endpoints c_1, c_{2L} [12]

would be their own anti-particles according to the theory, and therefore considered Majorana fermions. Perhaps these will be discovered in some future high-energy experiment, although with the lamented demise of the Large Hadron Collider, this prospect may be indefinitely postponed.

In solid-state physics, there is a well-studied quasiparticle called the *exciton*, which is a bound state of an electron and electron hole. Excitons have been studied in insulators, some liquids, and importantly, semiconductors. Conventional excitons are bosons with integer spin, but under special circumstances within a superconductor, "zero modes, spin-1/2 'excitons' of very low (formally, zero) energy" [11] are theorized to occur. These *Majorana Zero Modes* are now the subject of intense research, as groups around the globe work to prove their existence.

3.1.2 Kitaev's Toy Model

In 2001, Kitaev showed that unpaired Majorana quasiparticles could be localized at the endpoints of a "quantum wire" in close proximity to a superconductor [12]. He presents a "toy" model, which illustrates the conditions under which these unpaired Majoranas could be created. (Subsequent research described below attempts to implement this "quantum wire" using a semi-conducting nanowire, so here I use "nanowire," "semi-conducting wire," and "quantum wire" interchangeably). Consider a nanowire which constrains a series of spin-1/2 fermions to a one-dimensional line. Assume the wire contains L sites, which can either be occupied by a fermion or vacant, and that the wire is located very near to a superconductor (similar to Fig. 3.2(a)). Because Majoranas are their own anti-particle,

and so in a sense they constitute "half" of an ordinary fermion, when they are paired at the same site they combine to form an ordinary fermion. Stated another way, ordinary fermions can be decomposed into two Majoranas.

The Hamiltonian that governs the evolution of this system depends on several tunable physical parameters: The tunneling strength, or *hopping amplitude*, w; The induced superconducting gap, or *pairing potential*, $|\Delta|$; and the *chemical potential*, μ. In the simple case where $w = |\Delta| = 0$ and $\mu < 0$ which occurs when there is no superconduction and no tunneling strength, the Hamiltonian reduces to

$$H_1 = \frac{i}{2}(-\mu)\sum_j c_{2j-1}c_{2j},$$

where c_i are the Majorana operators. It can be seen that the Majorana pairs are grouped so each pair occupies a single fermion site: $(c_1, c_2), (c_3, c_4), ..., (c_{2L-1}, c_{2L})$ (as in Fig. 3.1(a)). However, in the case where $w = |\Delta| > 0$ and $\mu = 0$, the Hamiltonian becomes

$$H_1 = iw\sum_{j=1}^{L-1} c_{2j}c_{2j+1},$$

where the Majorana pairing is now *across* the sites: $(c_2, c_3), (c_4, c_5), ..., (c_{L-2}, c_{L-1})$ (Fig. 3.1(b)). Note that sites c_1 and c_{2L} are absent from the Hamiltonian, and therefore not involved in the energy of the system. These endpoints can be combined to form a highly non-local, zero-energy fermion operator of form

$$d_{end} = (c_1 + ic_{2L})/2$$

. There are then two orthogonal, degenerate ground states, which can be used as topologically protected qubit states:

$$|0\rangle \text{, where } d_{end}|0\rangle = 0$$
$$|1\rangle = d_{end}^{\dagger}|0\rangle$$

The picture here is that when the parameters are right, the Cooper pairs within the superconductor drive the pairing of the virtual Majoranas within the semiconductor so that there is one leftover Majorana at each end of the wire. These do not show up in the

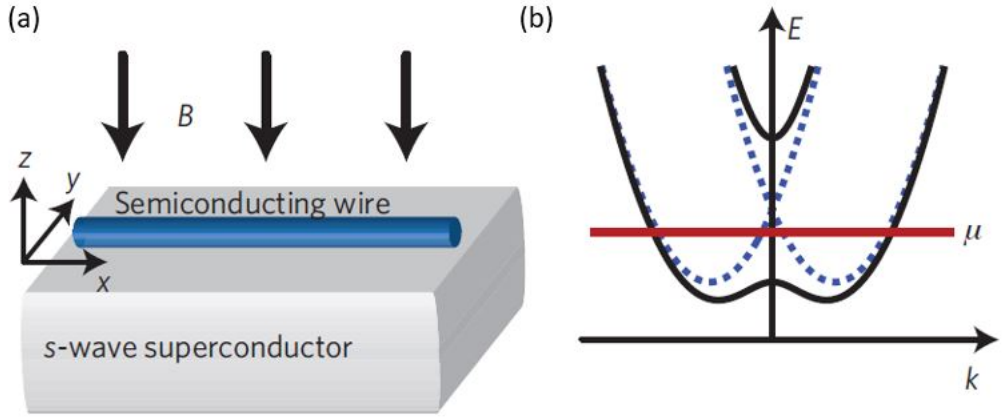

Figure 3.2: (a) Cartoon of nanowire in proximity to superconductor, in presence of magnetic field B; (b) Dashed line shows band structure of the wire with $B = 0$, and solid line shows band structure with $B > 0$. When the chemical potential, μ, lies within the band gap created by B, the pairing is driven across fermion sites, per (b) [13]

Hamiltonian, so they are zero-energy. These two quasiparticles taken together represent either a whole occupied site, or a whole unoccupied site, which correspond to the $|0\rangle$ and $|1\rangle$ qubit states.

3.1.3 Bringing the Toy to Life

To induce the pairing in the electrons, Kitaev's "toy" model assumes "triplet (p-wave) superconductivity in the three dimensional substrate," only spin up electrons, and the absence of spin-orbit interactions [12]. Today, p-wave superconductivity has not yet been conclusively demonstrated, and quantum wire with only spin $\uparrow$ electrons is an unobtainable idealization.

The same pairing can be accomplished in a "spin-orbit-coupled semiconducting wire semiconducting wire deposited on an s-wave superconductor," [13] with application of a magnetic field (Fig. 3.2(a)). S-wave superconductivity and semiconductor deposition are relatively well understood processes, and this configuration gives hope for a near-term implementation.

With $B = 0$, the semiconducting wire shows no band gap, as seen in dotted line of

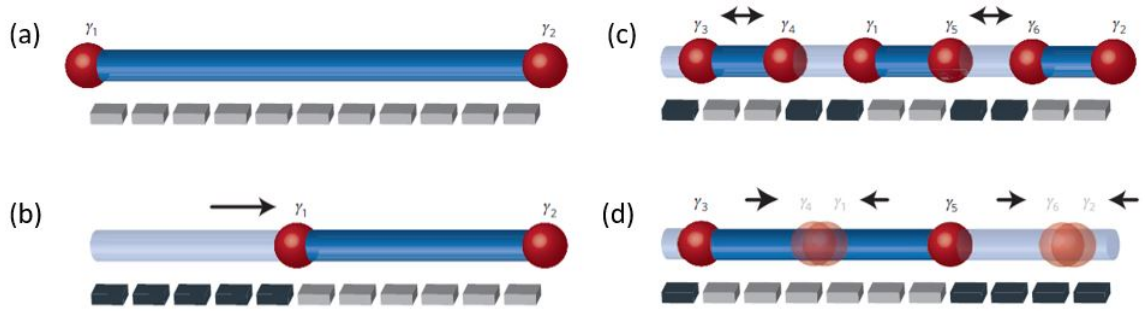

Figure 3.3: Creation, fusion, annihilation, and movement (a) "Keyboard" of voltage gates (light grey), to locally modify μ; (b) Sequentially applying gate voltage from left to right (darkened gates) moves Majorana operator γ_1 to the right, shortening the distance between endpoints; (c) Turning off gates 2 and 3 creates Majorana pair $\gamma_3\gamma_4$ from the vacuum; turning on gates 8 and 9 splits the pair $\gamma_1\gamma_2$ into $\gamma_1\gamma_5$ and $\gamma_6\gamma_2$; (d) γ_4 and γ_1 are fused into vacuum; γ_6 and γ_2 are fused to form an ordinary fermion.[13]

Fig. 3.2(b). As B is increased, an energy gap appears at momentum $k = 0$, shown by the solid curved line of the same figure. When the chemical potential μ is within the band gap, pairing in the superconductor drives the wire into the topological phase of Fig. 3.1(b). The ability to turn the Majoranas on and off by tuning μ electrically will become key in the discussion of gates that follows.

3.1.4 Create, Exchange, Fuse

To use Majorana qubits for computation, we need a mechanism to rotate and exchange them to create worldline braids. These are semiconductor and aluminum structures, cryogenically cooled to superconducting temperatures. There is no feasible way to mechanically move them about. Many different architectures and schemes for braiding appear in the literature. Here is one intuitive picture, to give a sense of the kinds of mechanisms under consideration.

As mentioned above, μ can be adjusted by applying a voltage. This effectively moves the horizontal line of Fig. 3.2(b) up or down, and changes the points of intersection with the lower band line. By adjusting μ downward so it is completely within the lower band and the lines no longer intersect, the wire is no longer driven into the topological phase. In this case, the Majoranas pair according to Fig. 3.1(a), fusing to become ordinary fermions.

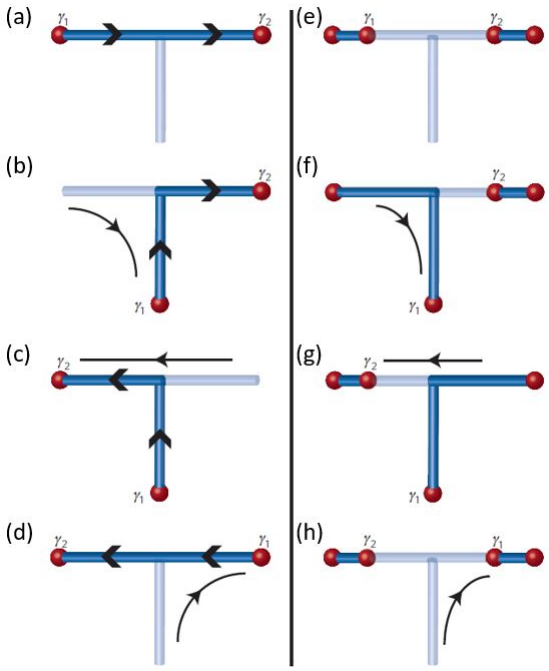

Figure 3.4: T-structure allows rotations and exchanges (a)-(d) γ_1 is adiabatically moved from the left end to the lowest point of the T, γ_2 takes its place, and γ_1 is moved to the right, enacting a counter-clockwise rotation; (e)-(h) γ_1 and its pair are moved to the lower branch of the T, γ_2 and its pair are moved to the left, and the pair with γ_1 moved to the right, enacting an exchange [13]

Local gates are expected to affect the bulk phase of the semiconductor locally. A series, or "keyboard" of gates (Fig. 3.3(a)), could be applied one by one to adiabatically move the Majorana locations along the wire (Fig. 3.3(b)). Turning off gates along a section of wire creates a Majorana pair from the vacuum, and turning on gates between a Majorana pair splits that pair in a reverse fusion operation (Fig. 3.3(c)). Majoranas are fused by moving them together (Fig. 3.3(d)), resulting in either the vacuum ($\gamma_4\gamma_1$), or a normal fermion ($\gamma_6\gamma_2$).

To achieve rotations and exchanges, we need a second dimension. By constructing a T structure of semiconducting wire lined with local voltage gates, Majorana end points can be moved off the main line, and rotations (Fig. 3.4(e)-(h)). Systems with many qubits could use ladder architectures, like many "H" structures connected end-to-end, to exchange and

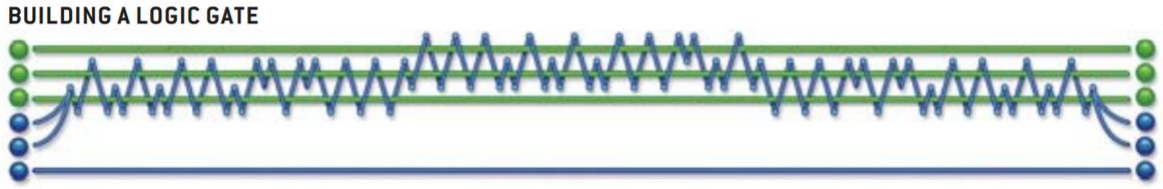

Figure 3.5: CNOT gate worldlines, showing braiding of two qubits made up of three anyons each, with about 90 exchanges, and redundancy to ensure accuracy to about 10^{-3}[14]

fuse non-adjacent Majorana pairs.

While the Majoranas are topologically protected states with indefinite coherence times, it will take many thousands of voltage gate operations to adiabatically move the Majorana endpoints to realize a usable logic gate. As illustrated above, a single exchange operation involves switching on and switching off many voltage gates. The requirement for adiabatic, smooth movement will impose a limit on the speed of operation. Algorithms made of many logical gates, such as the CNOT gate worldlines shown in Fig. 3.5, will require significant development to achieve.

3.2 Hardware in the Lab

Groups all over the world are working to realize physical implementations of MZM. This section presents several devices, from Microsoft Quantum Labs associated with Delft University of Technology, University of Copenhagen, and University of California at Santa Barbara. A few different architectures and gate structures are pictured and described below. These recent publications also provide analysis and evidence of Majorana signatures, but as of June 2020, there was not yet definitive proof that MZM states have actually been created.

3.2.1 Semiconducting-superconducting Devices and their Signatures

Recent publications from Microsoft Quantum associated labs in Delft and Copenhagen presented similar but notably different architectures, with strong evidence of Majoranas. These devices are constructed of epitaxially grown, hexagon semiconductor nanowires coated with aluminum, with gates fabricated with electron beam lithography. The experiments are

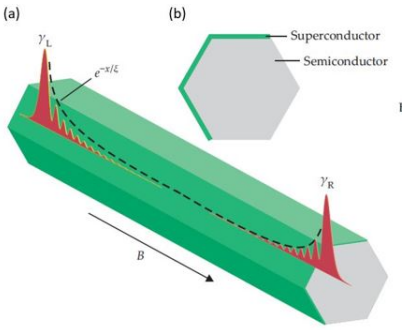

Figure 3.6: Detail of the implementation shown schematically in Fig.3.2(a). (a) Semiconductor-superconductor nanowire with theoretical MZM falling off exponentially at each endpoint; (b) Cross-section of nanowire, showing hexagonal semiconductor, typically indium arsenide or indium antimonide (grey), with thin plating of Al superconductor (green) [15]

.

conducted in dilution refrigerators at 20-50 mK.

Delft University As early as 2012, a team from Delft University published evidence that their indium antimonide semiconductor-superconductor quantum wire device produced MZMs at the endpoints [17]. In 2018, the same group published more refined results from a number of experiments [18, 16] based on devices which very closely implemented the architecture described in Section 3.1.3. Semiconductor "wire" of indium arsenide or indium antimonide is plated with a ˜10 nm layer of aluminum (Fig. 3.6). The various metallic gates (Fig. 3.7), made of chromium or gold, are used for tuning the chemical potential and other parameters, to drive the wire into a topological phase.

University of Copenhagen This chapter has focused on Kitaev's seminal idea, of coupling superconducting pairing into a semiconductor in close proximity, and driving unpaired Majoranas to the endpoints. However, there are other theoretical regimes in which Majoranas arise. For example, they may be bound in vortices in a topological superconductor. These could be created by coupling from a vortex in a regular superconductor to a topological insulator. In March of 2020, a group from University of Copenhagen published results

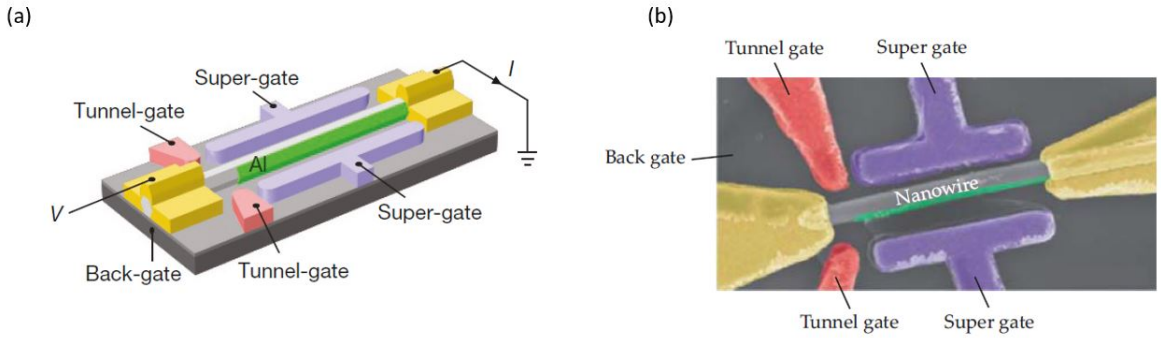

Figure 3.7: Integration of 3.6 into a real device (a) Schematic showing nanowire N, voltage source V and current measurement point, I. Zero-bias peaks are functions of conductance dI/dV [16]; (b) False-color scanning electron micrograph of the actual device. Overall image width is 3 μm [15]

that demonstrate a hybrid device, which utilizes a combination of both semiconductor-superconductor coupling, and bound vortex mechanisms [19]. The Copenhagen device uses indium arsenide semiconductor, and unlike in the Delft device, aluminum plating completely surrounds the hexagonal wire (Fig. 3.8(a)).

When magnetic flux is "threaded" or wound through the superconducting shell, MZMs arise at the endpoints of the wire.[2] The authors claim that this approach is similar in construction complexity to the non-hybrid devices, and has advantages such as that the aluminum coating protects the InAs from surface defects.

Zero bias peaks As we have been discussing, MZMs are expected to appear at the topological phase boundaries, namely the wire ends, or local to a control gate. The theory similarly predicts that MZMs should be detectable in the tunneling conductance, dI/dV, as a *zero bias anomaly* (ZBA), or a *zero bias peak* (ZBP). Evidence of this signature was first reported in 2012 by the Delft group (Fig. 3.9(a)) [17], although a number of more more conventional explanations were proposed, such as the Kondo effect,antilocalization, and reflectionless tunneling [20].

[2]It is not immediately clear what "flux-induced winding of the superconducting phase" means, given that superconductors reject magnetic flux.

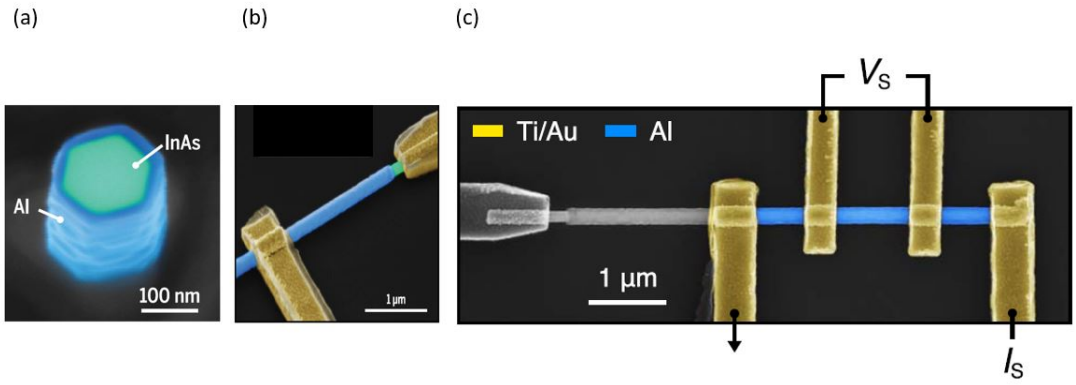

Figure 3.8: (a) Cross-section of indium arsenide semiconductor wire completely plated in superconducting aluminum; (b) Detail of device; (c) Entire device, showing the gates where V and I are applied, for generation of dI/dV conductance plots. [19]

Since then, a series of breakthroughs in the techniques of epitaxial growth of the Al superconductor directly onto the semiconductor, improvements in microfabrication, and deeper knowledge of the system parameters, have significantly reduced disorders at the superconductor-semiconductor interface, and led to crisp measurement of the ZBP. It is now understood that the ZBP height is quantized at $2e^2/h$ [21]. One by one, the alternative explanations for the ZBP have been eliminated, and the evidence for the existence of MZMs is growing stronger.

3.3 Future of Majorana Zero Mode Research

3.3.1 Immediate Next Steps

Nonetheless, significant work and basic science remain to be done, before the hope of TQC can be realized. Zhang et. al. [21] recommend a number of device configurations and investigations, which may become technically feasible in the near-term, and which are stepping stones to realizing non-Abelian braiding statistics and revealing the underlying physics. The six experiments are:

1. *Peak-to-dip transition in quantized Majorana conductance* Addition of a *tunnel gate* will enable extension of ZBP measurement, and distinguishing between MZM and

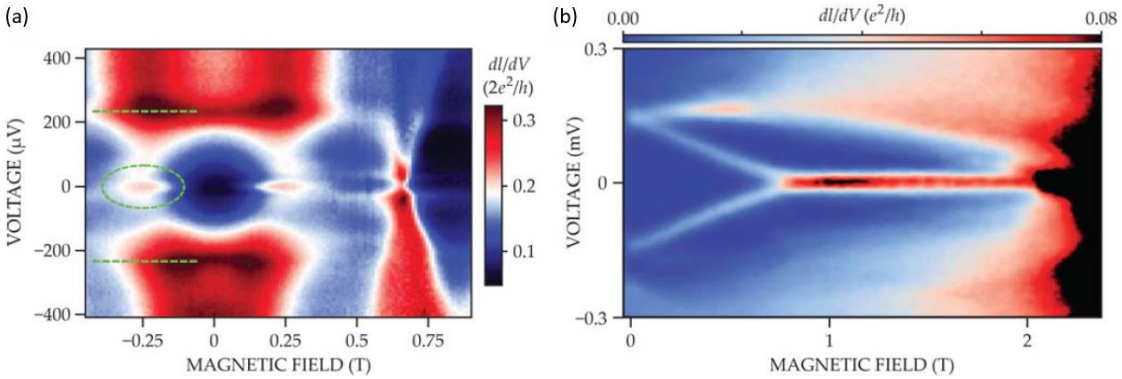

Figure 3.9: Zero bias peak (ZBP) or zero bias anomaly (ZBA) in the conductance dI/dV of two devices. (a) The 2012 device of [17] showing ZBA emerging within the superconducting gap (green oval); (b) Pronounced ZBA evident in similar conductance plot for coupled quantum-dot hybrid-nanowire device in 2016[22] (adapted from [15]).

trivial Andreev bound states (ABS), or partially separated Andreev bound states (ps-ABS) (not pictured).

2. *Non-local Majorana gate effect* (Fig. 3.10(a)) Addition of a *local gate* enables local tuning of the chemical potential, and movement of the Majorana state in real space, as pictured previously in Fig. 3.3(b).

3. *Correlation and three-terminal Majorana device* (Fig. 3.10(b)) This three-terminal device allows "detection of non-local crossed Andreev reflection processes," or independent current measurment from the electrodes at each endpoint of the nanowire (if the circuitry at left and right ends is replaced by ammeters).

4. *Majorana T-shape device for local density of states* (Fig. 3.10(c)) This T-shape structure can be used to detect local density of states within the wire bulk. It is likely addition of the T branching will introduce inhomogeneity in the wire bulk, and potentially create trivial Andreev bound states. So successful implementation of configurations (including the two below) with this type of T junction will depend on experimental innovation.

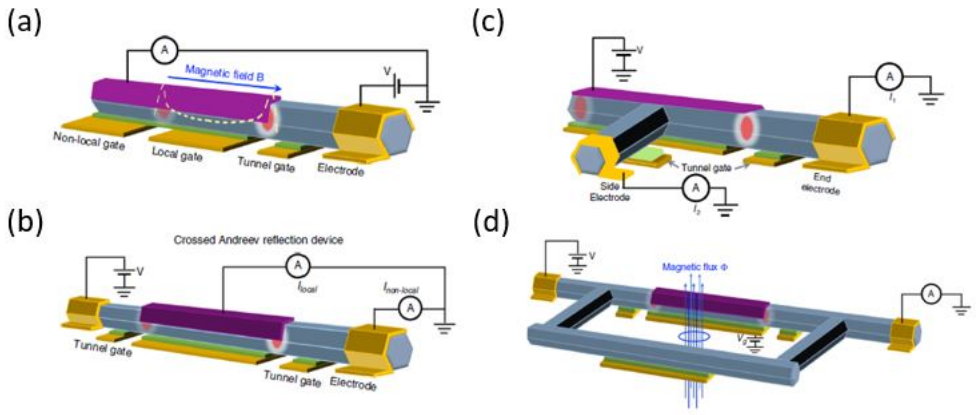

Figure 3.10: Four proposed device configurations for near-term experiments. (a) "Peak-to-dip transition in quantized Majorana conductance"; (b) "Non-local Majorana gate effect"; (c) "Majorana T-shape device for local density of states"; (d) "Majorana-Fu teleportation". [21]

.

5. *Majorana-Fu teleportation*(Fig. 3.10(d)) This interferometer structure may be used to study the non-local phase feature of the MZMs.

6. *Topological Kondo effect* This H shaped structure "will demonstrate that four Majorana zero modes can non-locally form a topological degeneracy, which is the basis of a topological qubit" (not pictured).

These experiments will drive our understanding of the physics, and the microfabrication techniques, for years into the future.

3.3.2 The Road Ahead

It is evident from the "Next Steps" experiments mentioned above that there are many years of work ahead to verify MZMs are actually being formed, and develop the ability to control them with local gates. The state of the devices and results of the Delft and Copenhagen teams published in 2020 show marked improvement from the 2012 effort, but the state of the art is proving the materials and the theory, not yet constructing qubits, let alone scaling

them to working computers. The MZM nanowire devices of today may be at the stage of Fig. 3.2(a), not yet even at Fig. 3.3(a). To achieve the kind of fidelity required to implement actual logic gates like Fig. 3.5.

In the short term, research will be focused on deeper understanding of the physics of the semiconductor-superconductor interface, that will lead to proof of MZMs, better measurement and characterization of the ZBP, and understanding of the toplogical and non-topological phase spaces [23]. It may be that functioning universal quantum computers can be built on the templates discussed above.

On the other hand, it could be that as we learn more about how topological superconductors and these semiconductor-superconductor interfaces, more complex and subtle physics may be discovered that eclipse Majorana modes for computation and simulation. For example, *Parafermions* are "generalizations of Majorana modes where the non-interacting nanowire is replaced with a fractional quantum Hall edge state" [23]. Parafermions would obey more complex non-Abelian fusion rules, and potentially implement quantum gates with fewer exchanges than MZMs. There is reason to hope that these states may turn out to be able to simulate the physics of black holes, or to test the hypotheses of super symmetry, as our understanding of the physics improves. The current work in characterizing the two-dimensional interfaces and arising MZM boundary states is a prerequisite for such future investigations.

Quantum computing and its promise of quantum speedup may enable calculations and simulations that could never be possible with conventional computers. But challenges with coherence and accuracy inhibit progress. Topological quantum computing solves these deep problems by exploiting topologically protected states that are inherently impervious to decoherence. Of the many potential topological architectures, MZMs have enjoyed significant research focus and have excellent prospects to be used as qubits for universal quantum computation in the mid-term. As these applications are pursued, theoretical and experimental advances are not only driving development of the building blocks of QC, but also exposing esoteric and exotic fundamental physics.

BIBLIOGRAPHY

[1] R. P. Feynman. Simulating physics with computers. *Int. J. Theor. Phys.*, 21, 1982.

[2] M. Le Bellac. *Quantum Information and Quantum Computation.* Cambridge University Press, 2006.

[3] Z. D. Romaszko, S. Hong, M. Siegele, R. K. Puddy, F. R. Lebrun-Gallagher, S. Weidt, and W. K. Hensinger. Engineering of microfabricated ion traps and integration of advanced on-chip features. *Nat. Rev. Phys.*, 2:285–299, 2020.

[4] B.B. Blinov. Class notes, phys 427: Lecture 10 and lecture 12. *University of Washington, PHYS 427*, 2016.

[5] P. Krantz, M. Kjaergaard, F. Yan, T. P. Orlando, S. Gustavsson, and W. D. Oliver. A quantum engineer's guide to superconducting qubits. *Appl. Phys. Rev.*, 6, 2019.

[6] F. Arute, K. Arya, and R. et. al. Babbush. Quantum supremacy using a programmable superconducting processor. *Nat.*, 574:505–510, 2019.

[7] H.-S. et. al. Zhong. Quantum computational advantage using photons. *Sci.*, 10.1126/science.abe8770, 2020.

[8] J. K. Pachos. *Introduction to Topological Quantum Computation.* Cambridge University Press, 2012.

[9] https://www.merriam webster.com/dictionary/topology, accessed 14-Nov-2020.

[10] R. Shankar. *Principles of Quantum Mechanics, 2nd Ed.* Springer, 1994.

[11] F. Wilczek. Majorana returns. *Nat. Phys.*, 5:614–8, 2009.

[12] A. Y. Kitaev. Unpaired majorana fermions in quantum wires. *Phys.-Usp.*, 44, 2001.

[13] J. Alicea1, Y. Oreg, G. Refael, F. von Oppen, and M. P. A Fisher. Non-abelian statistics and topological quantum information processing in 1d wire networks. *Nat. Phys.*, 7, 2011.

[14] G. P. Collins. Computing with quantum knots. *Sci. Amer.*, 294-4, 2006.

[15] R. Aguado and L. P. Kouwenhoven. Majorana qubits for topological quantum computing. *Phys. Today*, 73:44–50, June 2020.

[16] H. et. al. Zhang. Quantized majorana conductance. *Nat.*, 556, 2018.

[17] V. Mourik, K. Zuo, S. M. Frolov, S. R. Plissard, E. P. A. M. Bakkers, and L. P. Kouwenhoven. Signatures of majorana fermions in hybrid superconductor-semiconductor nanowire devices. *Sci.*, 336, 2012.

[18] Ö. Gü, H. Zhang, J. D. S. Bommer, M. W. A. de Moor, D. Car, S. R. Plissard, E. P. A. M Bakkers, Geresdi, K. Watanabe, T. Taniguchi, and L. P. Kouwenhoven. Ballistic majorana nanowire devices. *Nat. Nanotech.*, 13:192–7, 2018.

[19] S. Vaitiekėnas, G. W. Winkler, B. Van Heck, T Karzig, M.-T. Deng, K. Flensberg, and C. M. Marcus. Flux-induced topological superconductivity in full-shell nanowires. *Sci.*, 367:1442, 2020.

[20] R. Mark Wilson. Evidence for majorana fermions in a nanowire. *Phys. Today*, 65:14, June 2012.

[21] H. Zhang, D. E. Liew, M. Wimmer, and L. P. Kouwenhoven. Next steps of quantum transport in majorana nanowire devicess. *Nat. Comm.*, 10:5128–7, 2019.

[22] M. T. Deng, S. Vaitiekėnas, E. B. Hansen, J. Danon, M. Leijnse, K. Flensberg, Nygård J., P. Krogstrup, and C. M. Marcus. Majorana bound state in a coupled quantum-dot hybrid-nanowire system. *Sci.*, 354:1557–62, 2016.

[23] S.M. Frolov, M.J. Manfra, and J.D. Sau. Topological superconductivity in hybrid devices. *Nat. Phys.*, 16:718–724, 2020.

[24] G. J. Milburn. *The Feynman Processor*. Perseus Books, 1998.

[25] Born M. Born H. Trans. Born B. Einstein, A. *The Born-Einstein Letters: correspondence between Albert Einstein and Max and Hedwig Born from 1916 to 1955*. Walker and Company, 1971.

[26] A. Einstein, B. Podolsky, and N. Rosen. Can quantum-mechanical description of physical reality be considered complete? *Phys. Rev.*, 47:777–780, 1935.

[27] J.F. Lilieholm, N. Vasileios, A. Kato, K.C. Fu, and B.B. Blinov. Photon-mediated entanglement scheme between a zno semiconductor defect and a trapped yb ion. *Appl. Phys. Lett.*, 17, 2020.

[28] N. R. Ayukaryana, M. H. Fauzi, and E. H. Hasdeo. The quest and hope of majorana zero modes in topological superconductor for fault-tolerant quantum computing: An introductory overview. *The 4th International Seminar on Metallurgy and Materials (ISMM) 2020 Indonesian Institute of Sciences, arXiv:2009.07764v2, accessed 6-Dec-2020*, 2020.

[29] N. Read. Topological phases and quasiparticle braiding. *Phys. Today*, 65:38–43, July 2012.

[30] S. D. Sarma, M. Freedman, and C. Nayak. Majorana zero modes and topological quantum computation. *npj Quant. Inf.*, 1:15001, 2015.

VITA

Martin Caspe holds a BS degree in Physics from The Evergreen State College, MSEE and MBA degrees from University of Washington, and is a licensed Mechanical Engineer. His career has spanned product engineering of electronic systems, program management, purchasing, and procurement engineering in the Commercial Vehicle and Medical Device industries.

He welcomes your comments to `mcaspe@uw.edu`.